RSC Advances

PAPER

View Article Online
View Journal | View Issue

Check for updates

Cite this: *RSC Adv.*, 2017, **7**, 43826

Fabrication of methylammonium bismuth iodide through interdiffusion of solution-processed BiI_3/CH_3NH_3I stacking layers†

Huijia Wang,[ab] Jianhua Tian,[a] Kejian Jiang,[*b] Yu Zhang,[ab] Haochen Fan,[b] Jinhua Huang,[b] Lian-ming Yang,[b] Bo Guan[b] and Yanlin Song[*b]

Received 27th June 2017
Accepted 3rd September 2017

DOI: 10.1039/c7ra07123j

rsc.li/rsc-advances

Methylammonium bismuth iodide ($MA_3Bi_2I_9$) perovskite, has been deposited on a mesoporous TiO_2 film with high homogeneousity and coverage through interdiffusion of solution-processed BiI_3/CH_3NH_3I stacking layers, resulting in higher power conversion efficiency in the perovskite solar cell as compared with that prepared using a conventional one-step solution method.

Open Access Article. Published on 11 September 2017. Downloaded on 12/5/2025 3:03:39 AM.
This article is licensed under a Creative Commons Attribution 3.0 Unported Licence.

During the past few years, organic–inorganic hybrid perovskite materials, typically $CH_3NH_3PbI_3$, have been widely studied as an efficient active layer in solar cells due to their low cost, high light absorption capability, superior electron/hole mobility and facile solution processibility.[1–5] Great attention has been focused on improving the thin film fabrication, developing alternate solar cell architectures, and exploring the charge-transfer mechanism of the materials. By now, over 20% power conversion efficiencies (PCE) have been reported.[6] In view of the low cost materials and the simple production process, the perovskite photovoltaics will probably compete with the traditional inorganic counterparts. However, the lead element in the materials is very toxic, potentially resulting in persistent environmental pollution. Following the development of the lead perovskites, the less toxic tin counterparts (such as $CH_3NH_3SnI_3$) were reported, and PCEs of ~6% were achieved.[7] However, this class of materials suffers from serious stability problem, and processing and characterization of the devices were usually performed in nitrogen gas atmosphere to avoid the quick degradation of the tin perovskite. Thus, it is necessary to explore other lead-free perovskites with stable processibility and high photovoltaic performance. Among lead-free organic–inorganic hybrid perovskites, bismuth organo-halide compounds such as methylammonium bismuth iodide ($(CH_3)_3Bi_2I_9$) (MBI) have emerged as a possible candidate for photovoltaic applications due to their lower toxicity and environmental impact.[8–20]

Similar to the lead perovskites, a quality MBI film is a critical factor for achieving high efficient photovoltaic performance. Following the processing procedure of the lead perovskite films, the one-step solution method was usually employed for the deposition of MBI, where both the BiI_3 and CH_3NH_3I were dissolved in a polar solvent and deposited by spin coating. The resulting MBI film, however, usually present poor morphology with poor homogeneity and low coverage, mainly due to rapid crystallization of MBI from solution. Recently, gas-assisted one-step solution method was reported for the deposition of a dense and smooth MBI layer owing to rapid nucleation and crystallization, affording a PCE of 0.082%.[8] For controlling the crystallization, antisolvent-assisted crystallization and saturated vapor crystallization routes were employed for the deposition of MBI films.[9] In addition, it was reported that high quality MBI films could be obtained using *N*-methyl-2-pyrrolidone (NMP) as a morphology controller used in the MBI–DMF solution to control the rate of crystallization.[10] Recently, two-step method was explored for fabrication of smooth and continuous $(CH_3NH_3)_3Bi_2I_9$ layer in an inverted planar heterojunction solar cell with a PCE of 0.39%, where a dense and flat BiI_3 thin film was first prepared by thermal evaporation, and followed by solution coating of MAI and thermal annealing.[11] Different from the two-step method, in this work, both the BiI_3 and CH_3NH_3I were separately spin coated on a porous TiO_2 substrate, and the resulting BiI_3/CH_3NH_3I stacking layers were transformed into ($(CH_3)_3Bi_2I_9$) (MBI) through solid-state interdiffusion reaction. It should be noted that this method was successfully used for the fabrication of the lead perovskite solar cells by Huang and other's groups.[21,22] Here, the morphology of MBI film was strongly related to the concentration of MAI solution used. With optimization of the concentration, a homogeneous MBI film can be achieved with high surface coverage, and the resulting device exhibited a PCE of 0.29%.

The deposition process of $MA_3Bi_2I_9$ using two-step solution method is illustrated in Scheme 1. For the deposition, ~400 nm mesoporous TiO_2 film was first prepared on FTO glass substrate coated with ~30 nm TiO_2 blocking layer, and then 0.8 M BiI_3

[a]*School of Chemical Engineering and Technology, Tianjin University, Tianjin 300072, P. R. China*

[b]*Key Laboratory of Green Printing, Institute of Chemistry, Chinese Academy of Sciences, Beijing 100190, P. R. China. E-mail: kjjiang@iccas.ac.cn; ylsong@iccas.ac.cn*

† Electronic supplementary information (ESI) available. See DOI: 10.1039/c7ra07123j

This journal is © The Royal Society of Chemistry 2017

Open Access Article. Published on 11 September 2017. Downloaded on 12/5/2025 3:03:39 AM.
This article is licensed under a Creative Commons Attribution 3.0 Unported Licence.

solution in DMF was spin coated on the film, followed by coating of MAI solution. Finally, the stacked layers were transformed to $MA_3Bi_2I_9$ by thermal annealed at 100 °C for 1 h in glove box. The detailed procedures were shown in ESI.†

First, we investigated the morphological evolution of MBI film prepared by the two-step deposition method with various concentrations of MAI solutions (3, 6, 10 and 20 mg ml^{-1}). Fig. 1a shows SEM surface image of the BiI_3 film, where 0.8 M BiI_3 solution in DMF was spin-coated on a porous TiO_2 substrate. Besides the infiltration within the porous film, an over layer of the BiI_3 formed with plate shape, homogeneously dispersed on the whole surface of TiO_2 film. From the inset, we observed that the BiI_3 plates with size of ~300 nm lie flat on the film, in combination with uniformly distributed naked TiO_2 substrates. With the second coating of MAI solution with various concentrations and the interdiffusion reaction, the BiI_3 was converted into MBI and the surface images were shown in Fig. 1c–f. For comparison, the conventional one-step method was employed for the deposition of MBI film. As shown in Fig. 1b, the MBI solution was filled in the meso-TiO_2 film, and excess solution formed sharp-edged plate-like crystals, standing up-right on the TiO_2 surface with poor surface coverage, mainly due to uncontrolled crystallization of MBI from solution by the one-step method. The MBI morphology is in accordance with that previously reported with the same method.[19] When prepared using the two-step method, the resulting MBI changed drastically in structure. Following the morphology of starting precursor BiI_3, plate-like crystals of MBI lie flat on the TiO_2 surface with high coverage, as shown in Fig. 1c–f. Especially, we observed the coverage of the MBI was clearly improved with the increase of concentrations from 3 mg ml^{-1} and 6 mg ml^{-1}. The improvement can arise from quick nucleation rate and high crystallization at the higher concentration of MAI. The trend can be further revealed for the films formed at higher concentrations (10 and 20 mg ml^{-1}), as shown in Fig. 1e and f, where both the films exhibited much higher coverage by stacked MBI plates with smaller sizes of 300 nm, as compared with sizes of ~1 μm for the films formed at lower concentrations (3 and 6 mg ml^{-1}). The stacked and uneven MBI morphology could be bad for charge transfer in the photovoltaic devices.[23,24] Thus, we focused on investigation of the MBI film formed at the concentration of 6 mg ml^{-1} below.

For further checking the conversion and distribution of MBI within the porous TiO_2 film, the elemental distribution maps of Bi and I were recorded by EDX scan of the cross-sectional FESEM images. As shown in Fig. S1, 2 and Table S1,† I and Bi were homogeneously distributed within the porous TiO_2 film

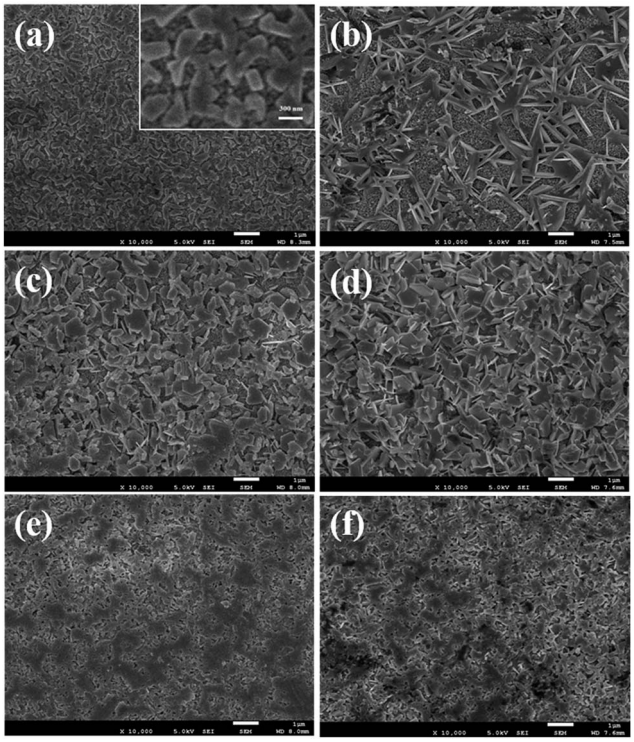

Fig. 1 Top surface SEM images of BiI_3 (a), one-step solution MBI (b), and two-step MBI prepared with various concentration of MAI: 3 mg ml^{-1} (c), 6 mg ml^{-1} (d), 10 mg ml^{-1} (e), and 20 mg ml^{-1} (f) on mesoporous TiO_2 films.

with the atom ratio of 4.3 : 1, closely with the value of 4.5 : 1 for MBI ($MA_3Bi_2I_9$), while the ratio is 2.6 : 1 for pristine BiI_3 (Fig. S3 and Table S2†). The results demonstrate that the two-step method is well suitable for the homogeneous deposition of MBI within a mesoporous TiO_2 film.

Fig. 2 shows UV-vis and PL spectra of BiI_3 and corresponding MBI film. For comparison, the absorption spectrum of MBI film prepared by the one-step method was included. The spin-coated BiI_3 film showed a broad absorption response ranged from 300 to 700 nm with the photoluminescence spectra centered at 1.80 eV, consistent with the reported results.[11] For the MBI films generated by the one-step or two-step method, the same absorption profiles can be observed with absorption edge at about 560 nm. The absorption of the later is clearly higher than that of the former, which could be related to higher coverage of the MBI film prepared by the two-step method, as shown in Fig. 2. The photoluminescence spectra of the MBI were recorded

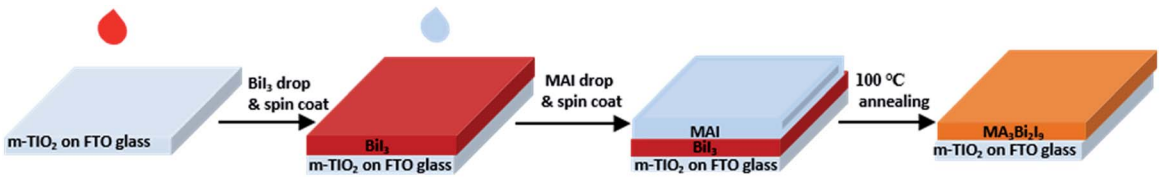

Scheme 1 Fabrication procedure of $MA_3Bi_2I_9$ on a mesoporous TiO_2 film through solution deposition and thermal annealing of BiI_3/MAI stacking layer.

Open Access Article. Published on 11 September 2017. Downloaded on 12/5/2025 3:03:39 AM.
This article is licensed under a Creative Commons Attribution 3.0 Unported Licence.

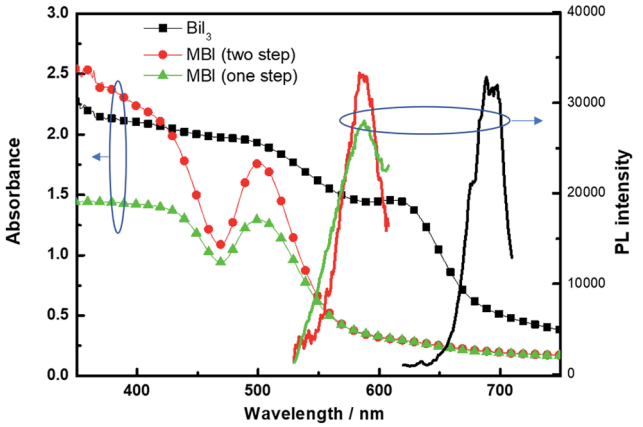

Fig. 2 UV-vis absorption and PL spectra of BiI_3, and MBI.

with peak at 2.21 eV, consistent with the value reported previously.[12]

Fig. 3 shows the XRD patterns of the BiI_3 and the corresponding MBI on soda-lime glasses coated with a porous TiO_2 layer. The deposited BiI_3 film showed typical diffraction peaks at $2\theta = 12.78$, 13.49, and 41.56°, corresponding to the (003), (113), and (300) lattice planes of hexagonal structured BiI_3 (JCPDS card no. 7-269).[19] After the transformation, no peaks for BiI_3 remained, while new diffraction peaks appear, which well match with the literature values of a hexagonal space group $P6_3/mmc$ MBI perovskite. In addition, XRD patterns were recorded for the MBI films from different concentrations of MAI, as shown in Fig. S4,† and all the peaks in the samples were assigned to the MBI and substrate TiO_2. For the one-step MBI, the same peaks were observed with comparable peak intensity. For excluding the effect from the glass substrate and TiO_2 scaffold, the MBI perovskite was also deposited on a quartz glass substrate using the two-step method. As shown in Fig. S5,† only peaks at 12.84°, 16.58°, and 24.82° were observed for (101), (004), and (006) planes of the MBI crystal. The results indicated that the TiO_2 scaffold strongly affected the crystal orientation during the growth. In order to assess the impact of the MBI films on the photovoltaic performance as light absorber in complete solar cells, we fabricate and characterize mesoscopic solar cells with the MBI films prepared with various MAI concentrations (3, 6, 10 and 20 mg ml^{-1}). The MBI absorber is sandwiched between a porous TiO_2 layer as the n-type electron collection layer, and 2,2(7,7(-tetrakis-(*N*,*N*-di-*p*-methoxyphenylamine)9,9(-spirobifluorene))) (spiro-OMeTAD) as the p-type hole collection layer. Fig. 4 shows schematic illustration and energy level diagram of the device. As shown in Table 1, for the MBI film prepared with MAI at concentration of 3 mg ml^{-1}, the resulting device gave the average power conversion efficiency (PCE) of 0.21%, with an open circuit voltage (V_{oc}) of 562 mV, a short-circuit current density (J_{sc}) of 0.93 mA cm^{-2}, and fill factor (FF) of 0.41. With increasing the concentration to 6 mg ml^{-1}, all the parameters were clearly improved with higher PCE of 0.27% (V_{oc}: mV, J_{sc}: 1.06 mA cm^{-2}, and FF: 0.43). With further increasing the concentration (10 and 20 mg ml^{-1}), however, we observed the PCE decreased clearly. The change in PCE can be related to the morphological evolution of the MBI films with various concentrations of MAI, as discussed above. For comparison, the MBI perovskite was prepared by the one-step method, the resulting device gave an average PCE of 0.14% with a V_{oc} of 554 mV, a J_{sc} of 0.62 mA cm^{-2}, and a FF of 0.39. The value in PCE is only half of that of the counterpart prepared by the two-step method. The higher PCE for the latter is reflected in all the performance parameters including J_{sc}, V_{oc}, and FF, which could be related to the striking contrast in their morphologies observed above. The high coverage of the MBI obtained for the latter can prevent shunting path between the two charge collecting layers, which is well known to be responsible for the higher fill factor and open-circuit voltage.[23] Moreover, the high coverage can efficiently collect the incident photons and generate high J_{sc}. The statistics of photovoltaic performance for devices by one step method and two step method with different concentrations of MBI's were provided in Fig. S6.†

In order to understand the relationship between the films and charge transport behavior in the devices, we performed electrochemical impedance spectroscopy (EIS) measurements on these devices over the frequency range of 10 mHz to 2 MHz under simulated AM 1.5G (100 mW cm^2 irradiance). As shown in Fig. S7,† the large arcs for both the one-step and two-step devices are displayed at the low-frequency region, associated with the recombination resistance (R_{rec}) at the $MA_3Bi_2I_9/TiO_2$ interface. The larger arc for the two-step device means high recombination resistance, and thus gave higher photovoltaic performance as compared with the one-step device.

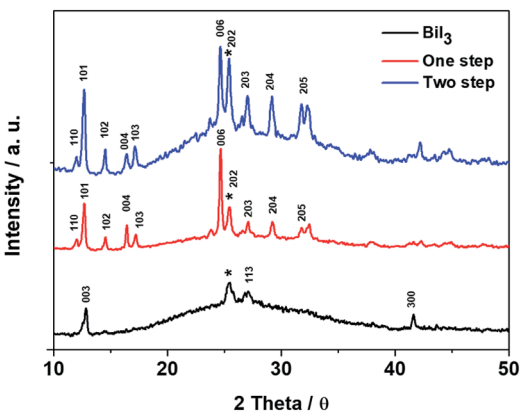

Fig. 3 XRD patterns of BiI_3 and MBI-deposited on mesoporous TiO_2 films (* for TiO_2).

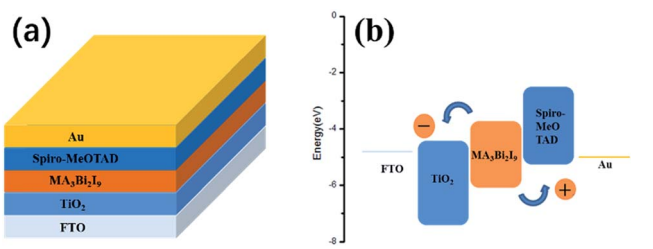

Fig. 4 Schematic illustration (a) and energy level diagram (b) of devices.

This journal is © The Royal Society of Chemistry 2017

Open Access Article. Published on 11 September 2017. Downloaded on 12/5/2025 3:03:39 AM.
This article is licensed under a Creative Commons Attribution 3.0 Unported Licence.

Table 1 The average photovoltaic performances with six parallel samples

	J_{sc}/mA cm^{-2}	V_{oc}/mV	FF	PCE/%
3 mg ml^{-1}	0.93 ± 0.08	562 ± 20	0.41 ± 0.09	0.21 ± 0.03
6 mg ml^{-1}	1.06 ± 0.10	604 ± 23	0.42 ± 0.07	0.27 ± 0.04
10 mg ml^{-1}	1.05 ± 0.11	554 ± 20	0.41 ± 0.10	0.23 ± 0.09
20 mg ml^{-1}	0.78 ± 0.09	562 ± 22	0.38 ± 0.12	0.16 ± 0.07
One step	0.62 ± 0.08	554 ± 21	0.37 ± 0.12	0.14 ± 0.10

Fig. 5a shows *I–V* curves for the best performing devices by the one-step and two-step methods, respectively, measured under simulated AM1.5G irradiation. Fig. 5b shows the incident photon-to-current conversion efficiency (IPCE) for the best-performing two-step device. The spectral response ranged from 350 to 600 nm, in accordance with the absorption spectrum of the MBI film, indicating that the MBI contributed to the photocurrent. In addition, the integration of the IPCE spectrum over the solar emission yields AM 1.5 photocurrent of 1.15 mA cm^{-2}, in excellent agreement with the measured J_{sc} value, indicating that the spectral mismatch between our simulator and the true AM 1.5 solar emission is small.

The hysteresis behavior is an important issue for the perovskite solar cells, which has been observed in many kinds of perovskite solar cells. Here, both the *J–V* curves for the two-step device almost overlapped for the forward and reverse scanning with 100 mV s^{-1} (Fig. S8†). In addition, the *J–V* curves were also recorded by reverse scanning with scanning rate ranging from 25 to 200 mV s^{-1} (Fig. S9†), and the curves show weak dependence with the scanning rate, especially at high rates between 50 to 200 mV s^{-1}. The results demonstrated that the two-step device had ignorable hysteresis behavior.

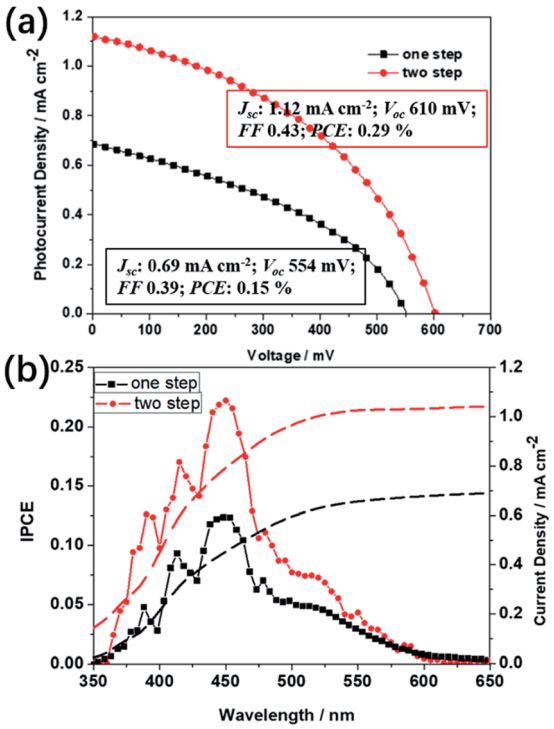

Fig. 5 (a) *I–V* curves for the best performing devices by the one-step and the two-step method, respectively, measured under simulated AM1.5G irradiation. (b) Corresponding IPCEs.

Conclusions

In this letter, methylammonium bismuth iodide (MBI) perovskite was deposited on a mesoporous TiO_2 film by two-step solution deposition, followed by interdiffusion of solution-processed BiI_3/MAI stacking layers. The morphology of the MBI film was strongly related to the concentration of MAI solution. Compared with the conventional one-step solution method, the two-step method led to higher homogeneity and coverage of the MBI on the TiO_2 film, and accordingly resulted in higher power conversion efficiencies in the corresponding MBI-based perovskite solar cells.

Conflicts of interest

There are no conflicts to declare.

Acknowledgements

This work was supported by the 973 Program (No. 2013CB933004), the National Nature Science Foundation of China (Grant No. 61405207, 21174149, 51473173, 91433202 and 21221002), and the "Strategic Priority Research Program" of Chinese Academy of Sciences (Grant No. XDA09020000 and XDB12010200).

Notes and references

1 A. Kojima, K. Teshima, Y. Shirai and T. Miyasaka, *J. Am. Chem. Soc.*, 2009, **131**, 6050.
2 H.-S. Kim, C.-R. Lee, J.-H. Im, K.-B. Lee, T. Moehl, A. Marchioro, S.-J. Moon, R. Humphry-Baker, J.-H. Yum, J.-E. Moser, M. Grätzel and N.-G. Park, *Sci. Rep.*, 2012, **2**, 591.
3 M. Liu, M. B. Johnston and H. J. Snaith, *Nature*, 2013, **501**, 395.
4 J. Burschka, N. Pellet, S.-J. Moon, R. Humphry-Baker, P. Gao, M. K. Nazeeruddin and M. Grätzel, *Nature*, 2013, **499**, 316.
5 M. A. Green, A. Ho-Baillie and H. J. Snaith, *Nat. Photonics*, 2014, **8**, 506.
6 W. Chen, Y. Z. Wu, Y. F. Yue, J. Liu, W. J. Zhang, X. D. Yang, H. Chen, E. B. Bi, I. Ashraful and M. Grätzel, *Science*, 2015, **350**, 944.
7 N. K. Noel, S. D. Stranks, A. Abate, C. Wehrenfennig, S. Guarnera, A.-A. Haghighirad, A. Sadhanala, G. E. Eperon, S. K. Pathak, M. B. Johnston, A. Petrozza, L. M. Herz and H. J. Snaith, *Energy Environ. Sci.*, 2014, **7**, 3061.
8 T. Okano and Y. Suzuki, *Mater. Lett.*, 2017, **191**, 77.
9 S. S. Mali, H. Kim and D. H. Kim, *ChemistrySelect*, 2017, **2**, 1578.
10 A. Kulkarni, T. Singh, M. Ikegami and T. Miyasaka, *RSC Adv.*, 2017, **7**, 9456.

Open Access Article. Published on 11 September 2017. Downloaded on 12/5/2025 3:03:39 AM.
This article is licensed under a Creative Commons Attribution 3.0 Unported Licence.

11 C. Ran, Z. Wu, J. Xi, F. Yuan, H. Dong, T. Lei, X. He and X. Hou, *J. Phys. Chem. Lett.*, 2017, **8**, 394.
12 B. W. Park, B. Philippe, X. Zhang, H. Rensmo, G. Boschloo and E. M. J. Johansson, *Adv. Mater.*, 2015, **27**, 6806.
13 K. Eckhardt, V. Bon, J. Getzschmann, J. Grothe, F. M. Wisser and S. Kaskel, *Chem. Commun.*, 2016, **52**, 3058.
14 R. L. Z. Hoye, R. E. Brandt, A. Osherov, V. Stevanovic, S. D. Stranks, M. W. B. Wilson, H. Kim, A. J. Akey, J. D. Perkins, R. C. Kurchin, J. R. Poindexter, E. N. Wang, M. G. Bawendi, V. Bulović and T. Buonassisi, *Chem.–Eur. J.*, 2016, **22**, 2605.
15 M. Abulikemu, S. Ould-Chikh, X. Miao, E. Alarousu, B. Murali, G. O. N. Ndjawa, J. Barbe, A. E. Labban, A. Amassian and S. D. Gobbo, *J. Mater. Chem. A*, 2016, **4**, 12504.
16 M. Lyu, J. H. Yun, M. Cai, Y. Jiao, P. V. Bernhardt, M. Zhang, Q. Wang, A. Du, H. Wang, G. Liu and L. Wang, *Nano Res.*, 2016, **9**, 692.
17 S. Öz, J. C. Hebig, E. Jung, T. Singh, A. Lepcha, S. Olthof, F. Jan, Y. Gao, R. German, P. H. M. Loosdrecht, K. Meerholze, T. Kirchartz and S. Mathur, *Sol. Energy Mater. Sol. Cells*, 2016, **158**, 195.
18 T. Singh, A. Kulkarni, M. Ikegami and T. Miyasaka, *ACS Appl. Mater. Interfaces*, 2016, **8**, 14542.
19 X. Zhang, G. Wu, Z. Gu, B. Guo, W. Liu, S. Yang, T. Ye, C. Chen, W. Tu and H. Chen, *Nano Res.*, 2016, **9**, 2921.
20 A. J. Lehner, D. H. Fabini, H. A. Evans, C. A. Hebert, S. R. Smock, J. Hu, H. Wang, J. W. Zwanziger, M. L. Chabinyc and R. Seshadri, *Chem. Mater.*, 2015, **27**, 7137.
21 Z. Xiao, C. Bi, Y. Shao, Q. Dong, Q. Wang, Y. Yuan, C. Wang, Y. Gao and J. Huang, *Energy Environ. Sci.*, 2014, **7**, 2619.
22 J.-H. Im, I.-H. Jang, N. Pellet, M. Grätzel and N.-G. Park, *Nat. Nanotechnol.*, 2014, **9**, 907.
23 W. Nie, H. Tsai, R. Asadpour, J.-C. Blancon, A. J. Neukirch, G. Gupta, J. J. Crochet, M. Chhowalla, S. Tretiak, M. A. Alam, H.-L. Wang and A. D. Mohite, *Science*, 2015, **347**, 522.
24 C. Bi, Q. Wang, Y. Shao, Y. Yuan, Z. Xiao and J. Huang, *Nat. Commun.*, 2015, **6**, 7747.

 This journal is © The Royal Society of Chemistry 2017